SYNERGISTIC EFFECTS OF LOADING SEQUENCE AND INTERFACE WEAR ON DAMAGE EVOLUTION IN FIBER REINFORCED CERAMIC-MATRIX COMPOSITES

Li Longbiao

College of Civil Aviation, Nanjing University of Aeronautics and Astronautics
No.29 Yudao St., Nanjing 210016
Email: llb451@nuaa.edu.cn

Keywords: Ceramic-matrix composites (CMCs), Airworthiness, Damage evolution, Interface wear.

ABSTRACT

The synergistic effects of loading sequence and interface wear on the damage evolution in fiber-reinforced ceramic-matrix composites (CMCs) have been investigated. The shear-lag model combined with matrix cracking model, interface debonding criterion and interface wear model has been adopted to analyze the damage evolution in CMCs under different loading sequences. The relationships between damage parameters, i.e., the fatigue hysteresis loops, fatigue hysteresis dissipated energy, and matrix crack spacing, interface debonding and sliding, have been established. The effects of stress levels, matrix crack spacing, fiber volume fraction on the damage evolution of CMCs have been analysed. The fatigue hysteresis loops, fatigue hysteresis dissipated energy, and the interface slip lengths of cross-ply SiC/CAS composite have been predicted.

1 INTRODUCTION

Ceramic-matrix composites (CMCs) possess high strength-to-weight ratio at high temperatures, and are being designed and developed for hot section components in commercial aero engine [[1]]. General Electric and Rolls Royce are currently testing prototype exhaust and shroud components for the GE-CFM LEAP engine, the GE Passport 20 Engine and the Rolls Royce Trent 1000 engine. As new materials, the CMCs need to meet the airworthiness certification requirements, and it is necessary to analyze the degradation, damage and failure mechanisms subjected to cyclic fatigue loading at different testing conditions.

Upon unloading and subsequent reloading, the stress−strain hysteresis loops would develop due to frictional slip occurred along any interface debonded region [2, 3]. Holmes and Cho [4] performed an investigation on the fatigue loading history and microstructural damages on fatigue hysteresis loops and frictional heating of unidirectional CMCs at room temperature. The fatigue loading frequency, stress levels, stress ranges and matrix crack spacing all affect the area of fatigue hysteresis loops. The extent of specimen surface temperature rise is controlled by the relative slip distance of fibers within matrix. Reynaud [5] investigated the fatigue hysteresis loops evolution of two types of CMCs at elevated temperatures in inert atmosphere. First, the fatigue hysteresis loops area of 2D SiC/SiC composite increases with the increase of number of applied cycles due to interface thermal residual compressive stress. The second ceramic composite, [0/90] SiC/MAS−L, the fatigue hysteresis loops area decreases with the increase of cycle number due to interface radial thermal residual tensile stress. Steen and Valles [6] investigated the average slope, irreversible strain and width of loading/unloading hysteresis loops of 2D SiC/Al_2O_3 and 2D C/SiC composites under tensile, creep and fatigue tests at room and elevated temperatures. Mei and Cheng [7] investigated the cyclic loading/unloading tensile hysteresis behavior of needled, 2D, 2.5D and 3D C/SiC composites at room temperature. It was found that the increase in permanent strain and the decrease in stiffness were affected by fiber volume fraction in the loading direction. Fantozzi et al. [8] investigated the fatigue hysteresis behavior of bi− or multi−directional (cross−weave, cross−ply, 2.5D, $[0/+60/-60]_n$) with SiC or C long fibers reinforced SiC, MAS−L, Si−B−C or C matrix at room and elevated temperatures in inert or oxidation conditions. By assuming mechanical behavior of composites is mainly controlled by mechanical

behavior of longitudinal yarns, the fatigue hysteresis loops shape variations of these composites have been analyzed.

The objective of this paper is to investigate the synergistic effects of loading sequence and interface wear on the damage evolution in fiber-reinforced ceramic-matrix composites (CMCs). The shear-lag model combined with matrix cracking model, interface debonding criterion and interface wear model has been adopted to analyze the damage evolution in CMCs under different loading sequences. The relationships between damage parameters, i.e., the fatigue hysteresis loops, fatigue hysteresis dissipated energy, and matrix crack spacing, interface debonding and sliding, have been established. The effects of stress levels, matrix crack spacing, fiber volume fraction on the damage evolution of CMCs have been analysed. The fatigue hysteresis loops, fatigue hysteresis dissipated energy, and the interface slip lengths of cross-ply SiC/CAS composite have been predicted.

2 THEORETICAL ANALYSIS

If matrix multicracking and fiber/matrix interface debonding are present upon first loading to fatigue peak stress σ_{max}^{I}, the stress–strain hysteresis loops would develop as a result of energy dissipation through frictional slip between fibers and matrix upon unloading/reloading. After experiencing N cycles, the interface shear stress in the interface debonded region decreases from initial value τ_i to τ_f due to interface wear. When fatigue peak stress increases from σ_{max}^{I} to σ_{max}^{II}, the crack propagates along the fiber/matrix interface. The original interface debonded length at fatigue peak stress of σ_{max}^{I} is defined to be ξ, and the new interface debonded length at fatigue peak stress of σ_{max}^{II} is defined to be l_d. The shape, size and location of fatigue hysteresis loops depend upon the new stress level of σ_{max}^{II}, the interface debonding and frictional slip occurred in the new and original debonded region.

The fatigue peak stress σ_t, at which the interface completely slips relative to matrix in the interface debonded region upon unloading/reloading, is determined by Eq. (1).

$$\sigma_t = 2\frac{V_f E_c \tau_i}{\rho V_m E_m}\left[1+\sqrt{1+4\frac{V_m E_m E_f}{r_f E_c}\frac{\rho^2}{\tau_i^2}\zeta_d}\right]-\sigma_{min} \tag{1}$$

where V_f and V_m denote the fiber and matrix volume fraction, respectively; E_f, E_m and E_c denote the elastic modulus of fiber, matrix and composite, respectively; r_f denotes the fiber radius; ρ denotes the shear-lag model parameter; τ_i denotes the fiber/matrix interface shear stress; and ζ_d denotes the fiber/matrix interface debonded energy.

When $\sigma_{max}^{II} < \sigma_t$, the interface counter-slip length y upon unloading is affected by the interface debonding. The interface counter-slip length y, upon completely unloading, is equal to the interface debonded length l_d. The fiber slides completely relative to matrix in the interface debonded region unpon unloading/reloading. When $\sigma_t < \sigma_{max}^{II} < \sigma_b$, the interface counter-slip length y, upon completely unloading, is less than the interface debonded length l_d. The fiber slides partially relative to matrix in the interface debonded region upon unloading/reloading. The interface completely debonding stress σ_b is determined by Eq. (2).

$$\sigma_b = \frac{V_f E_c \tau_i}{\rho V_m E_m}\left[1+\rho\frac{l_c}{r_f}-\rho\left(1-\frac{\tau_f}{\tau_i}\right)\frac{2\xi}{r_f}+\sqrt{1+4\frac{V_m E_m E_f}{r_f E_c}\frac{\rho^2}{\tau_i^2}\zeta_d}\right] \tag{2}$$

When $\sigma_{max}^{II} > \sigma_b$, the interface completely debonds. The fatigue peak stress σ_p, at which the interface completely slips upon unloading/reloading, is determined by Eq. (3).

$$\sigma_p = 2\frac{V_f E_c}{V_m E_m}\frac{l_c}{r_f}\tau_i - 4\frac{V_f E_c}{V_m E_m}\frac{\xi}{r_f}\left(1-\frac{\tau_f}{\tau_i}\right)\tau_i + \sigma_{min}^2 \tag{3}$$

When $\sigma_b < \sigma_{max}^{II} < \sigma_p$, the interface counter-slip length y upon completely unloading, is less than the half matrix crack spacing $l_c/2$. The fiber slides partially relative to matrix in the interface debonded region upon unloading/reloading. When $\sigma_p < \sigma_{max}^{II}$, the interface counter-slip length y upon completely

unloading, is equal to the half matrix crack spacing $l_c/2$. The fiber slides completely relative to matrix in the interface debonded region upon unloading/reloading.

Based on the interface frictional slip cases between fibers and matrix, the fatigue hysteresis loops under multiple loading stress levels can be divided into four different cases, i.e., (1) the interface partially debonds, and fiber completely slips relative to matrix; (2) the interface partially debonds, and fiber partially slips relative to matrix; (3) the interface completely debonds, and fiber partially slips relative to matrix; and (4) the interface completely debonds, and fiber completely slips relative to matrix in the interface debonded region upon unloading/reloading.

The unloading and reloading stress–strain relationships for interface partially debonding, are determined by Eqs. (4) and (5).

$$\begin{aligned}\varepsilon_{\mathrm{c\_pu}} &= \frac{2\sigma l_{\mathrm{d}}}{V_{\mathrm{f}}E_{\mathrm{f}}l_{\mathrm{c}}} + \frac{2\tau_{\mathrm{f}}}{r_{\mathrm{f}}E_{\mathrm{f}}l_{\mathrm{c}}}\xi^2 + \frac{4\tau_{\mathrm{f}}}{r_{\mathrm{f}}E_{\mathrm{f}}l_{\mathrm{c}}}\xi\left(l_{\mathrm{d}}-\xi\right) + \frac{4\tau_{\mathrm{i}}}{r_{\mathrm{f}}E_{\mathrm{f}}l_{\mathrm{c}}}\left(y-\xi\right)^2 - \frac{2\tau_{\mathrm{i}}}{r_{\mathrm{f}}E_{\mathrm{f}}l_{\mathrm{c}}}\left(2y-\xi-l_{\mathrm{d}}\right)^2 \\ &+ \frac{2\sigma_{\mathrm{fo}}}{E_{\mathrm{f}}l_{\mathrm{c}}}\left(\frac{l_{\mathrm{c}}}{2}-l_d\right) + \frac{2r_{\mathrm{f}}}{\rho E_{\mathrm{f}}l_{\mathrm{c}}}\left[\frac{V_{\mathrm{m}}}{V_{\mathrm{f}}}\sigma_{\mathrm{mo}} + \frac{2\tau_{\mathrm{f}}}{r_{\mathrm{f}}}\xi + \frac{2\tau_{\mathrm{i}}}{r_{\mathrm{f}}}\left(2y-\xi-l_{\mathrm{d}}\right)\right] \\ &\times\left[1-\exp\left(-\rho\frac{l_{\mathrm{c}}/2-l_{\mathrm{d}}}{r_{\mathrm{f}}}\right)\right] - \left(\alpha_{\mathrm{c}}-\alpha_{\mathrm{f}}\right)\Delta\mathrm{T}\end{aligned} \tag{4}$$

$$\begin{aligned}\varepsilon_{\mathrm{c\_pr}} &= \frac{2\sigma}{V_{\mathrm{f}}E_{\mathrm{f}}l_{\mathrm{c}}}l_{\mathrm{d}} - \frac{4\tau_{\mathrm{f}}}{r_{\mathrm{f}}E_{\mathrm{f}}l_{\mathrm{c}}}z^2 + \frac{2\tau_{\mathrm{f}}}{r_{\mathrm{f}}E_{\mathrm{f}}l_{\mathrm{c}}}\left(2z-\xi\right)^2 - \frac{4\tau_{\mathrm{f}}}{r_{\mathrm{f}}E_{\mathrm{f}}l_{\mathrm{c}}}\left(2z-\xi\right)\left(l_{\mathrm{d}}-\xi\right) + \frac{4\tau_{\mathrm{i}}}{r_{\mathrm{f}}E_{\mathrm{f}}l_{\mathrm{c}}}\left(y-\xi\right)^2 \\ &- \frac{2\tau_{\mathrm{i}}}{r_{\mathrm{f}}E_{\mathrm{f}}l_{\mathrm{c}}}\left(2y-\xi-l_{\mathrm{d}}\right)^2 + \frac{2\sigma_{\mathrm{fo}}}{E_{\mathrm{f}}l_{\mathrm{c}}}\left(\frac{l_{\mathrm{c}}}{2}-l_{\mathrm{d}}\right) + \frac{2r_{\mathrm{f}}}{\rho E_{\mathrm{f}}l_{\mathrm{c}}}\left[\frac{V_{\mathrm{m}}}{V_{\mathrm{f}}}\sigma_{\mathrm{mo}} - \frac{2\tau_{\mathrm{f}}}{r_{\mathrm{f}}}\left(2z-\xi\right) + \frac{2\tau_{\mathrm{i}}}{r_{\mathrm{f}}}\left(2y-\xi-l_{\mathrm{d}}\right)\right] \\ &\times\left[1-\exp\left(-\rho\frac{l_{\mathrm{c}}/2-l_{\mathrm{d}}}{r_{\mathrm{f}}}\right)\right] - \left(\alpha_{\mathrm{c}}-\alpha_{\mathrm{f}}\right)\Delta\mathrm{T}\end{aligned} \tag{5}$$

The unloading and reloading stress–strain relationships for interface completely debonding, are determined by Eqs. (6) and (7).

$$\varepsilon_{\mathrm{c\_fu}} = \frac{\sigma}{V_{\mathrm{f}}E_{\mathrm{f}}} - \frac{2\tau_{\mathrm{f}}}{r_{\mathrm{f}}E_{\mathrm{f}}l_c}\xi^2 + \frac{2\tau_{\mathrm{f}}}{r_{\mathrm{f}}E_{\mathrm{f}}}\xi + \frac{4\tau_{\mathrm{i}}}{r_{\mathrm{f}}E_{\mathrm{f}}l_{\mathrm{c}}}\left(y-\xi\right)^2 - \frac{2\tau_{\mathrm{i}}}{r_{\mathrm{f}}E_{\mathrm{f}}l_{\mathrm{c}}}\left(2y-\xi-\frac{l_{\mathrm{c}}}{2}\right)^2 - \left(\alpha_{\mathrm{c}}-\alpha_{\mathrm{f}}\right)\Delta\mathrm{T} \tag{6}$$

$$\begin{aligned}\varepsilon_{\mathrm{c\_fr}} &= \frac{\sigma}{V_{\mathrm{f}}E_{\mathrm{f}}} - \frac{4\tau_{\mathrm{f}}}{r_{\mathrm{f}}E_{\mathrm{f}}l_{\mathrm{c}}}z^2 + \frac{2\tau_{\mathrm{f}}}{r_{\mathrm{f}}E_{\mathrm{f}}l_{\mathrm{c}}}\left(2z-\xi\right)^2 - \frac{4\tau_{\mathrm{f}}}{r_{\mathrm{f}}E_{\mathrm{f}}l_{\mathrm{c}}}\left(2z-\xi\right)\left(y-\xi\right) + \frac{4\tau_{\mathrm{i}}}{r_{\mathrm{f}}E_{\mathrm{f}}l_{\mathrm{c}}}\left(y-\xi\right)^2 \\ &- \frac{4\tau_{\mathrm{f}}}{r_{\mathrm{f}}E_{\mathrm{f}}l_{\mathrm{c}}}\left(2z-\xi\right)\left(\frac{l_{\mathrm{c}}}{2}-y\right) - \frac{2\tau_{\mathrm{i}}}{r_{\mathrm{f}}E_{\mathrm{f}}l_{\mathrm{c}}}\left(2y-\xi-\frac{l_{\mathrm{c}}}{2}\right)^2 - \left(\alpha_{\mathrm{c}}-\alpha_{\mathrm{f}}\right)\Delta\mathrm{T}\end{aligned} \tag{7}$$

Under cyclic fatigue loading, the area associated with the stress–strain hysteresis loops is the energy lost during corresponding cycle, which is defined as,

$$S = \int_{\sigma_{\min}}^{\sigma_{\max}}\left[\varepsilon_{\mathrm{c}}^{\mathrm{unload}}\left(\sigma\right) - \varepsilon_{\mathrm{c}}^{\mathrm{reload}}\left(\sigma\right)\right]d\sigma \tag{8}$$

3 DISCUSSIONS

The fatigue hysteresis loops, fatigue hysteresis loss energy and interface slip of cross-ply SiC/CAS II composite under multiple fatigue peak stress levels have been analyzed. The basic material properties are given by: V_{f}=35%, E_{f}=190GPa, E_{m}=90GPa, r_{f}=7.5μm, α_{f}=3.1×10^{-6}/°C, α_{m}=4.5×10^{-6}/°C, $\Delta\mathrm{T}$ **=** −1000°C, ζ_{d}=0.2J/m^2.

3.1 Effect of fiber volume content

The effect of fiber volume content, i.e., V_{f}=35% and 40%, on the fatigue hysteresis loss energy, interface debonded length $2l_{\mathrm{d}}/l_{\mathrm{c}}$ and unloading interface counter-slip length y/l_{d} under multiple fatigue peak stress levels of $\sigma_{\max}^{1}$ =100 MPa and $\sigma_{\max}^{2}$ =180 MPa is illustrated in Fig. 1. When fiber volume content is V_{f}=35%, the fatigue hysteresis loss energy increases from 3.4 kPa when interface shear

stress is τ_i=50 MPa to 26.4 kPa when interface shear stress is τ_i=6.5 MPa, as shown in Fig. 1(a), corresponding to interface slip Case 2, i.e., the interface partially debonds ($l_d<l_c/2$, i.e., A_1–B_1 part in Fig. 1(b)), and fiber slips partially relative to matrix in the interface debonded region ($y(\sigma_{min})<l_d$, i.e., A_1–B_1 part in Fig. 1(c)); and increases to 38.1 kPa when interface shear stress is τ_i=4.5 MPa, corresponding to interface slip Case 3, i.e., the interface completely debonds ($l_d=l_c/2$, i.e., B_1–C part in Fig. 1(b)), and fiber slips partially relative to matrix in the interface debonded region ($y(\sigma_{min})<l_d$, i.e., B_1–C_1 part in Fig. 1(c)); and increases to the peak value of 41.8 kPa when interface shear stress is τ_i=3.5 MPa, and decreases to 22 kPa when interface shear stress is τ_i=1 MPa, corresponding to interface slip Case 4, i.e., the interface completely debonds ($l_d=l_c/2$, i.e., B_1–C part in Fig. 1(b)), and fiber slips completely relative to matrix in the interface debonded region ($y(\sigma_{min})=l_d$, i.e., C_1–D part in Fig. 1(c)).

When fiber volume content is V_f=40%, the fatigue hysteresis loss energy increases from 2.1 kPa when interface shear stress is τ_i=50 MPa to 22.9 kPa when interface shear stress is τ_i=4.5 MPa, as shown in Fig. 1(a), corresponding to interface slip Case 2, i.e., the interface partially debonds ($l_d<l_c/2$, i.e., A_2–B_2 part in Fig. 1(b)), and fiber slips partially relative to matrix in the interface debonded region ($y(\sigma_{min})<l_d$, i.e., A_2–B_2 part in Fig. 1(c)); and increases to 29.5 kPa when interface shear stress is τ_i=3.5 MPa, corresponding to interface slip Case 3, i.e., the interface completely debonds ($l_d=l_c/2$, i.e., B_2–C part in Fig. 1(b)), and fiber slips partially relative to matrix in the interface debonded region ($y(\sigma_{min})<l_d$, i.e., B_2–C_2 part in Fig. 1(c)); and increases to the peak value of 32.9 kPa when interface shear stress is τ_i=2.5 MPa, and decreases to 20.5 kPa when interface shear stress is τ_i=1 MPa, corresponding to interface slip Case 4, i.e., the interface completely debonds ($l_d=l_c/2$, i.e., B_2–C part in Fig. 1(b)), and fiber slips completely relative to matrix in the interface debonded region ($y(\sigma_{min})=l_d$, i.e., C_2–D part in Fig. 1(c)).

With the increase of fiber volume content, the interface debonded length and interface slip lengths, i.e., unloading interface counter-slip length and reloading interface new-slip length, would decrease when interface partially and completely debonded, as shown in Figs. 1(b) and (c); the fatigue hysteresis loss energy decreases for interface slip Case 1 ~ 3; however, when the interface slip corresponds to Case 4, the fatigue hysteresis loss energy approaches the same value, as shown in Fig. 1(a). When fiber volume content increases, the range and extent of interface frictional slip between the fiber and the matrix in the interface debonded region would decrease when the interface slip corresponds to Case 1 ~ 3, leading to the decrease of fatigue hysteresis loss energy.

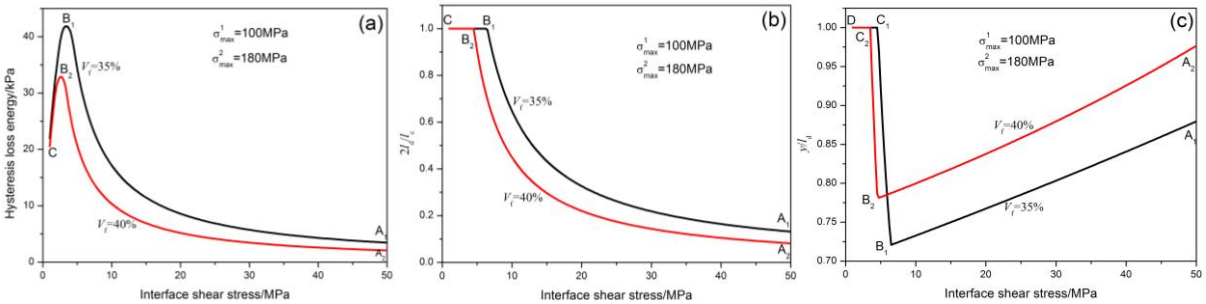

Fig.1. The effect of fiber volume content, i.e., V_f=35% and 40%, on (a) the fatigue hysteresis loss energy versus the interface shear stress; (b) the interface debonded length ($2l_d/l_c$) versus the interface shear stress; and (c) the unloading interface counter-slip length (y/l_d) versus the interface shear stress in the new interface debonded region under multiple loading fatigue peak stress levels of σ^1_{max} =100 MPa and σ^2_{max} =180 MPa with interface shear stress in the interface wear region of τ_f=1MPa.

3.2 Effect of matrix crack spacing

The effect of matrix crack spacing, i.e., $l_c=20r_f$ and $30r_f$, on the fatigue hysteresis loss energy, interface debonded length $2l_d/l_c$ and unloading interface counter-slip length y/l_d under multiple fatigue peak stress levels of σ^1_{max} =100 MPa and σ^2_{max} =180 MPa is illustrated in Fig. 2. When matrix crack spacing is $l_c=20r_f$, the fatigue hysteresis loss energy increases from 4.6 kPa when interface shear stress is τ_i=50 MPa to 25.9 kPa when interface shear stress is τ_i=8.8 MPa, as shown in Fig. 2(a),

corresponding to interface slip Case 2, i.e., the interface partially debonds ($l_d<l_c/2$, i.e., A_1–B_1 part in Fig. 2(b)), and fiber slips partially relative to matrix in the interface debonded region ($y(\sigma_{min})<l_d$, i.e., A–B_1 part in Fig. 2(c)); and increases to 37.2 kPa when interface shear stress is τ_i=6.1 MPa, as shown in Fig. 2(a), corresponding to interface slip Case 3, i.e., the interface completely debonds ($l_d=l_c/2$, i.e., B_1–C part in Fig. 2(b)), and fiber slips partially relative to matrix in the interface debonded region ($y(\sigma_{min})<l_d$, i.e., B_1–C_1 part in Fig. 2(c)); and increases to the peak value of 41.5 kPa when interface shear stress is τ_i=4.4 MPa, and decreases to 17.1 kPa when interface shear stress is τ_i=1 MPa, as shown in Fig. 2(a), corresponding to interface slip Case 4, i.e., the interface completely debonds ($l_d=l_c/2$, i.e., B_1–C part in Fig. 2(b)), and fiber slips completely relative to matrix in the interface debonded region ($y(\sigma_{min})=l_d$, i.e., C_1–D part in Fig. 2(c)).

When matrix crack spacing is $l_c=30r_f$, the fatigue hysteresis loss energy increases from 3.1 kPa when interface shear stress is τ_i=50 MPa to 25.8 kPa when interface shear stress is τ_i=5.9 MPa, as shown in Fig. 2(a), corresponding to interface slip Case 2, i.e., the interface partially debonds ($l_d<l_c/2$, i.e., A_2–B_2 part in Fig. 2(b)), and fiber slips partially relative to matrix in the interface debonded region ($y(\sigma_{min})<l_d$, i.e., A–B_2 part in Fig. 2(c)); and increases to 38.6 kPa when interface shear stress is τ_i=3.9 MPa, as shown in Fig. 2(a), corresponding to interface slip Case 3, i.e., the interface completely debonds ($l_d=l_c/2$, i.e., B_2–C part in Fig. 2(b)), and fiber slips partially relative to matrix in the interface debonded region ($y(\sigma_{min})<l_d$, i.e., B_2–C_2 part in Fig. 2(c)); and increases to the peak value of 42 kPa when interface shear stress is τ_i=3 MPa and decreases to 24 kPa when interface shear stress is τ_i=1 MPa, as shown in Fig. 2(a), corresponding to interface slip Case 4, i.e., the interface completely debonds ($l_d=l_c/2$, i.e., B_2–C part in Fig. 2(b)), and fiber slips completely relative to matrix in the interface debonded region ($y(\sigma_{min})=l_d$, i.e., C_2–D part in Fig. 2(c)).

With the increase of matrix crack spacing, the extent of interface debonding and interface frictional slip in the entire matrix crack spacing would decrease at the same interface shear stress when interface partially debonded, as shown in Figs. 2(b) and (c), and increases when interface completely debonded; the fatigue hysteresis loss energy decreases when interface partially debonded and increases when interface completely debonded at the same interface shear stress, as shown in Fig. 2(a). When matrix crack spacing increases, the extent of interface frictional slip between the fiber and the matrix in the interface debonded region would be affected by interface debonding, i.e., decreases when interface partially debonds, and increases when interface completely debonds.

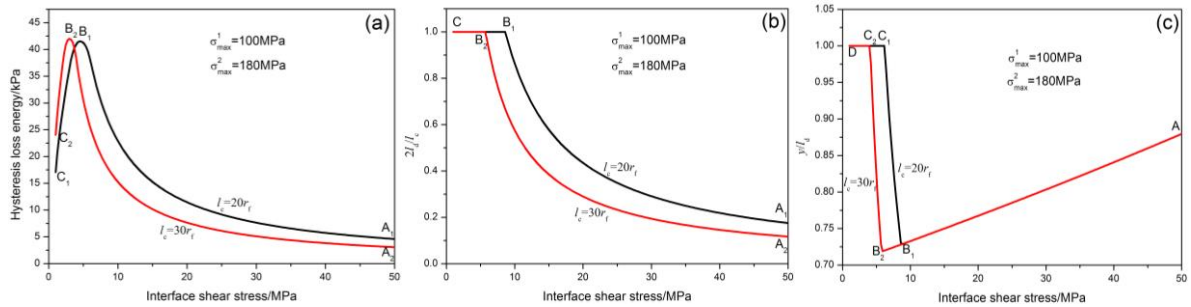

Fig.2. The effect of matrix crack spacing, i.e., $l_c=20r_f$ and $30r_f$ on (a) the fatigue hysteresis loss energy versus the interface shear stress; (b) the interface debonded length ($2l_d/l_c$) versus the interface shear stress; and (c) the unloading interface counter-slip length (y/l_d) versus the interface shear stress in the new interface debonded region under multiple loading fatigue peak stress levels of σ^1_{max} =100 MPa and σ^2_{max} =180 MPa with interface shear stress in the interface wear region of τ_f=1MPa.

3.3 Effect of stress range

The effect of stress range, i.e., $\Delta\sigma$=100 and 120 MPa, on the fatigue hysteresis loss energy, interface debonded length $2l_d/l_c$ and unloading interface counter-slip length y/l_d under multiple fatigue peak stress levels of σ^1_{max} =100 MPa and σ^2_{max} =180 MPa is illustrated in Fig. 3. When stress range is $\Delta\sigma$=100 MPa, the fatigue hysteresis loss energy increases from 0.59 kPa when interface shear stress is τ_i=50 MPa to 4.4 kPa when interface shear stress is τ_i=6.6 MPa, i.e., A_1–B_1 in Fig. 3(a), corresponding

to interface slip Case 2, i.e., the interface partially debonds ($l_d<l_c/2$, i.e., A–B part in Fig. 3(b)), and fiber slips partially relative to matrix in the interface debonded region ($y(\sigma_{min})<l_d$, i.e., A_1–B_1 part in Fig. 3(c)); and increases to 11.8 kPa when interface shear stress is τ_i=2.5 MPa, i.e., B_1–C_1 part in Fig. 3(a), corresponding to interface slip Case 3, i.e., the interface completely debonds ($l_d=l_c/2$, i.e., B–C part in Fig. 3(b)), and fiber slips partially relative to matrix in the interface debonded region ($y(\sigma_{min})<l_d$, i.e., B_1–C_1 part in Fig. 3(c)); and increases to the peak value of 12.9 kPa when interface shear stress is τ_i=2 MPa, i.e., C_1–D_1 part in Fig. 3(a), and decreases to 10.2 kPa when interface shear stress is τ_i=1 MPa, i.e., D_1–E_1 part in Fig. 3(a), corresponding to interface slip Case 4, i.e., the interface completely debonds ($l_d=l_c/2$, i.e., B–C part in Fig. 3(b)), and fiber slips completely relative to matrix in the interface debonded region ($y(\sigma_{min})=l_d$, i.e., C_1–D part in Fig. 3(c)).

When stress range is $\Delta\sigma$=120 MPa, the fatigue hysteresis loss energy increases from 1 kPa when interface shear stress is τ_i=50 MPa to 7.6 kPa when interface shear stress is τ_i=6.6 MPa, i.e., A_2–B_2 in Fig. 3(a), corresponding to interface slip Case 2, i.e., the interface partially debonds ($l_d<l_c/2$, i.e., A–B in Fig. 3(b)), and fiber slips partially relative to matrix in the interface debonded region ($y(\sigma_{min})<l_d$, i.e., A_2–B_2 in Fig. 3(c)); and increases to 17.1 kPa when interface shear stress is τ_i=2.9 MPa, i.e., B_2–C_2 part in Fig. 3(a), corresponding to interface slip Case 3, i.e., the interface completely debonds ($l_d=l_c/2$, i.e., B–C part in Fig. 3(b)), and fiber slips partially relative to matrix in the interface debonded region ($y(\sigma_{min})<l_d$, i.e., B_2–C_2 part in Fig. 3(c)); and increases to the peak value of 18.6 kPa when interface shear stress is τ_i=2.2 MPa, i.e., C_2–D_2 part in Fig. 3(a), and decreases to 13 kPa when interface shear stress is τ_i=1 MPa, i.e., D_2–E_2 part in Fig. 3(a), corresponding to interface slip Case 4, i.e., the interface completely debonds ($l_d=l_c/2$, i.e., B–C part in Fig. 3(b)), and fiber slips completely relative to matrix in the interface debonded region ($y(\sigma_{min})=l_d$, i.e., C_2–D part in Fig. 3(c)).

With the increase of stress range, the interface slip lengths, i.e., unloading interface counter-slip length and reloading interface new-slip length would increase when the interface partially and completely debonded as shown in Fig. 3(c); however, the interface debonded length l_d depend upon peak stress, which is not affected by stress range, as shown in Fig. 3(b); the fatigue hysteresis loss energy increases due to the increase of extent and range of interface frictional slip between the fiber and the matrix, as shown in Fig. 3(a).

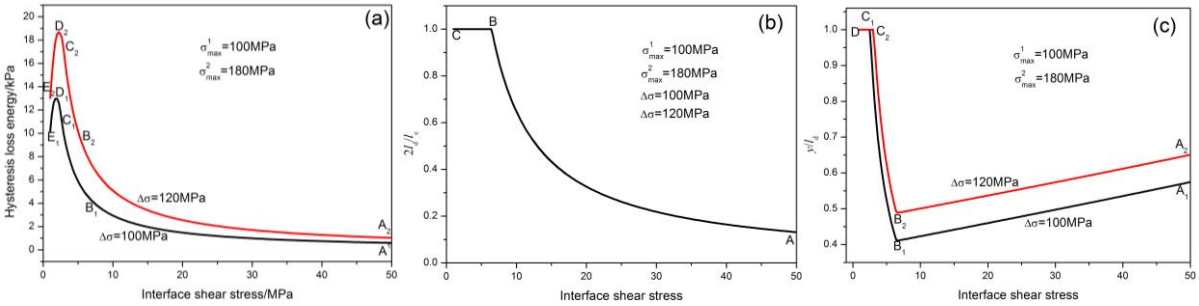

Fig.3. The effect of fatigue stress range, i.e., $\Delta\sigma$=100 and 120 MPa, on (a) the fatigue hysteresis loss energy versus the interface shear stress; (b) the interface debonded length ($2l_d/l_c$) versus the interface shear stress; and (c) the unloading interface counter-slip length (y/l_d) versus the interface shear stress in the new interface debonded region under multiple loading fatigue peak stress levels of σ_{max}^1 =100 MPa and σ_{max}^2 =180 MPa with interface shear stress in the interface wear region of τ_f=1MPa.

3.4 Effect of loading sequence

The effect of loading sequence, i.e., Case I: σ_{max}^1 =140 MPa, σ_{max}^2 =180 MPa and Case II: σ_{max}^1 =180 MPa, σ_{max}^2 =140 MPa on the fatigue hysteresis loss energy, interface debonded length $2l_d/l_c$ and unloading interface counter-slip length y/l_d is illustrated in Fig. 4. When loading sequence is Case I: σ_{max}^1 =140 MPa and σ_{max}^2 =180 MPa, the fatigue hysteresis loss energy increases from 3.5 kPa when interface shear stress is τ_i=50 MPa to 25 kPa when interface shear stress is τ_i=6.8 MPa, i.e., A_1–B_1 part in Fig. 4(a), corresponding to interface slip Case 2, i.e., the interface partially debonds ($l_d<l_c/2$, A_1–B_1 part in Fig. 4(b)), and fiber slips partially relative to matrix in the interface debonded

region ($y(\sigma_{min})<l_d$, A_1–B_1 part in Fig. 4(c)); and increases to 36.7 kPa when interface shear stress is τ_i=4.7 MPa, i.e., B_1–C_1 part in Fig. 4(a), corresponding to interface slip Case 3, i.e., the interface completely debonds ($l_d=l_c/2$, i.e., B_1–C part in Fig. 4(b)), and fiber slips partially relative to matrix in the interface debonded region ($y(\sigma_{min})<l_d$, B_1–C_1 part in Fig. 4(c)); and increases to the peak value of 40.7 kPa when interface shear stress is τ_i=3.4 MPa, i.e., C_1–D_1 part in Fig. 4(a), then decreases to 22 kPa when interface shear stress is τ_i=1 MPa, i.e., D_1–E_1 part in Fig. 4(a), corresponding to interface slip Case 4, i.e., the interface completely debonds ($l_d=l_c/2$, i.e., B_1–C part in Fig. 4(b)), and fiber slips completely relative to matrix in the interface debonded region ($y(\sigma_{min})=l_d$, C_1–D part in Fig. 4(c)).

When loading sequence is Case 2: σ^1_{max} =180 MPa and σ^2_{max} =140 MPa, the fatigue hysteresis loss energy increases from 1.8 kPa when interface shear stress is τ_i=50 MPa to 10.4 kPa when interface shear stress is τ_i=7.8 MPa, i.e., A_2–B_2 part in Fig. 4(a), corresponding to interface slip Case 2, i.e., the interface partially debonds ($l_d<l_c/2$, A_2–B_2 part in Fig. 4(b)), and fiber slips partially relative to matrix in the interface debonded region ($y(\sigma_{min})<l_d$, A_2–B_2 part in Fig. 4(c)); and increases to 21.9 kPa when interface shear stress is τ_i=3.7 MPa, i.e., B_2–C_2 part in Fig. 4(a), corresponding to interface slip Case 3, i.e., the interface completely debonds ($l_d=l_c/2$, i.e., B_2–C part in Fig. 4(b)), and fiber slips partially relative to matrix in the interface debonded region ($y(\sigma_{min})<l_d$, B_2–C_2 part in Fig. 4(c)); and increases to the peak value of 24.2 kPa when interface shear stress is τ_i=2.7 MPa, i.e., C_2–D_2 part in Fig. 4(a), then decreases to 16 kPa when interface shear stress is τ_i=1 MPa, i.e., D_2–E_2 part in Fig. 4(a), corresponding to interface slip Case 4, i.e., the interface completely debonds ($l_d=l_c/2$, i.e., B_2–C part in Fig. 4(b)), and fiber slips completely relative to matrix in the interface debonded region ($y(\sigma_{min})=l_d$, C_2–D part in Fig. 4(c)).

Compared with low-high peak stress loading sequence, i.e., $\sigma^1_{max} < \sigma^2_{max}$, the interface debonded length under high-low peak stress loading sequence, i.e., $\sigma^1_{max} > \sigma^2_{max}$, increases when interface partially debonded as shown in Fig. 4(b), and the interface slip lengths, i.e., unloading interface counter-slip length and reloading interface new-slip length, decreases when interface partially debonded due to the increase of interface debonded length, as shown in Fig. 4(c); the fatigue hysteresis loss energy under high-low peak stress loading sequence decreases for interface slip Case 1 ~ 4, as shown in Fig. 4(a).

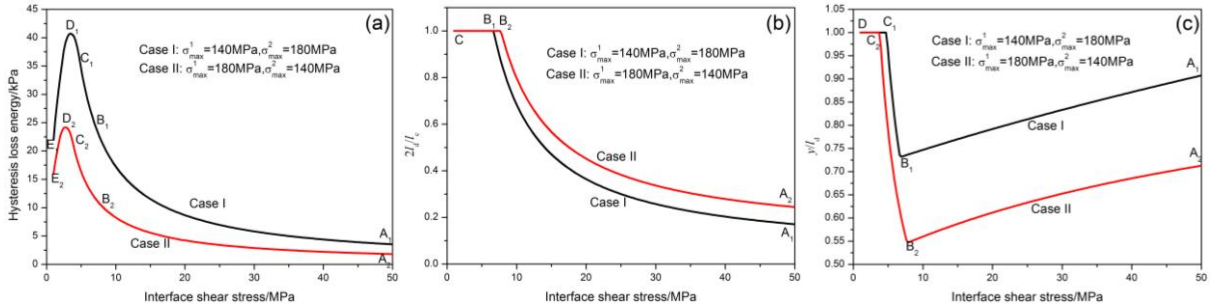

Fig.4. The effect of fatigue loading sequence, i.e., Case I: σ^1_{max} =140 MPa and σ^2_{max} =180 MPa; and Case II: σ^1_{max} =180 MPa and σ^2_{max} =140 MPa, on (a) the fatigue hysteresis loss energy versus the interface shear stress; (b) the interface debonded length ($2l_d/l_c$) versus the interface shear stress; and (c) the unloading interface counter-slip length (y/l_d) versus the interface shear stress in the new interface debonded region with interface shear stress in the interface wear region of τ_f=1MPa.

4 CONCLUSIONS

In this paper, the synergistic effects of loading sequence and interface wear on the damage evolution in fiber-reinforced ceramic-matrix composites (CMCs) have been investigated. Based on the fatigue damage mechanism of fiber slipping relative to matrix in the interface debonded region upon unloading/reloading, the unloading interface counter-slip length and reloading interface new-slip length are determined by fracture mechanics method. The fatigue hysteresis

loops models corresponding to different interface slip cases under multiple fatigue peak stress levels have been derived, i.e., (1) the interface partially debonds, and fiber slips completely relative to matrix; (2) the interface partially debonds, and fiber slips partially relative to matrix; (3) the interface completely debonds, and fiber slips partially relative to matrix; and (4) the interface completely debonds, and fiber slips completely relative to matrix in the interface debonded region upon unloading/reloading. The fatigue hysteresis loss energy and interface slip corresponding to single and multiple loading stress levels, different fiber volume content, matrix crack spacing, stress range and loading sequence have been investigated.

ACKNOWLEDGEMENTS

The work reported here is supported by the Natural Science Fund of Jiangsu Province (Grant No. BK20140813), and the Fundamental Research Funds for the Central Universities (Grant No. NS2016070).

REFERENCES

[1] R. Naslain, Design, preparation and properties of non-oxide CMCs for application in engines and nuclear reactors: an overview. *Composites Science and Technology*, **64**, 2004, pp. 155–170. (doi: 10.1016/S0266-3538(03)00230-6)

[2] A.G. Evans, F.W. Zok, R.M. McMeeking, Fatigue of ceramic matrix composites. *Acta metall. mater*. **43**, 1995, pp. 859–875. (doi: 10.1016/0956-7151(94)00304-Z)

[3] G. Camus, Modelling of the mechanical behavior and damage processes of fibrous ceramic matrix composites: application to a 2-D SiC/SiC. *International Journal of Solids and Structures*, **37**, 2000, pp. 919–942. (doi:10.1016/S0020-7683(99)00065-7)

[4] J.W. Holmes, C.D. Cho, Experimental observation of frictional heating in fiber-reinforced ceramics. *Journal of the American Ceramic Society* **75**, 1992, pp. 929–938. (doi:10.1111/j.1151-2916.1992.tb04162.x)

[5] P. Reynaud, Cyclic fatigue of ceramic-matrix composites at ambient and elevated temperatures. *Composites Science and Technology*, **56**, 1996, pp. 809–814. (doi:10.1016/0266-3538(96)00025-5)

[6] M. Steen, J.L. Valles, Unloading-reloading sequences and the analysis of mechanical test results. *Thermal and Mechanical Test Methods and Behavior of Continuous-Fiber Ceramic Composites*, ASTM STP 1309, American Society for Testing and Materials 1997.

[7] H. Mei, L.F. Cheng, Comparison of the mechanical hysteresis of carbon/ceramic-matrix composites with different fiber performs. *Carbon*, **47**, 2009, pp. 1034–1042. (doi: 10.1016/j.carbon.2008.12.025)

[8] G. Fantozzi, P. Reynaud, Mechanical hysteresis in ceramic matrix composites. *Materials Science and Engineering A* **521-522**, 2009, pp. 18–23. (doi: 10.1016/j.msea.2008.09.128)